



ChemComm

**Ni₂P Active Site Ensembles Tune Electrocatalytic Nitrate
Reduction Selectivity**

Journal:	<i>ChemComm</i>
Manuscript ID	CC-COM-04-2024-001834.R1
Article Type:	Communication

SCHOLARONE™
Manuscripts

COMMUNICATION

Ni₂P Active Site Ensembles Tune Electrocatalytic Nitrate Reduction Selectivity

Received 00th January 20xx,
Accepted 00th January 20xx

Emily Nishiwaki^a, Peter S. Rice^b, Ding-Yuan Kuo^a, Florence Y. Dou^a, Anthony Pyka^c, Bryce Reid^c, Hao A. Nguyen^a, Eric M. Stuve^c, Simone Raugel^b, Brandi M. Cossairt^{a*}

DOI: 10.1039/x0xx00000x

We demonstrate that active site ensembles on transition metal phosphides tune the selectivity of the nitrate reduction reaction. Using Ni₂P nanocrystals as a case study, we report a mechanism involving competitive co-adsorption of H* and NO_x* intermediates. A 100% Faradaic efficiency for nitrate reduction over hydrogen evolution is observed at -0.4 V, while NH₃ selectivity is maximized at -0.2 V vs. RHE.

Ammonia is an essential fertilizer for supporting global food demands.¹ It is produced industrially via the Haber-Bosch process, which combines gaseous nitrogen and hydrogen at high temperatures and pressures over an iron-based heterogeneous catalyst. However, the enormous scale of ammonia production and deployment has disrupted the nitrogen cycle. Imbalances of NO₃⁻ in wastewater and extraneous nitrous oxides emitted into the atmosphere from burning fossil fuels for H₂ production have resulted in ecosystem destruction and climate change.^{2,3} Anthropogenic disturbances to the nitrogen cycle motivate alternative ammonia generation methods that do not exacerbate these imbalances. One alternative is the electrocatalytic nitrate reduction reaction (NO₃RR), which can upcycle NO₃⁻ to NH₃.⁴ State-of-the-art catalysts usually include noble metals^{5–9}, but current electrocatalyst design research focuses on using earth-abundant metals to achieve similar current densities.^{10–13}

Several studies have proposed a NO₃RR mechanism that involves H* and NO_x* adsorption and a sequential deoxygenation-hydrogenation mechanism to convert NO₃⁻ to NH₃.^{14–16} With this knowledge, metal phosphides have been designed and demonstrated as selective NO₃RR electrocatalysts toward NH₃.^{17–25} We hypothesize that metal phosphides have active site ensembles of adjacent strongly and weakly H-binding sites.²⁶ On these surfaces, strongly bound H can hydrogenate

NO_x*, which can bind on a vacated site that only weakly adsorbs hydrogen.²⁷ Density functional theory (DFT) calculations have suggested that active site ensembles of strongly and weakly binding hydrogen sites are responsible for Ni₂P's HER activity.^{28–32} The importance of these ensembles has also been realized in more complex electrocatalytic reactions such as CO₂ electroreduction, where several metal phosphides have demonstrated the ability to form oxygenated hydrocarbons.^{33–37} The binary surfaces of metal phosphides result in an increased number of unique surface sites and a distribution of adsorbate-binding energetics, which enhance their ability to co-adsorb different species.

Thermal hydrogenation studies with Ni₂P and Ni nanocrystals showed Ni₂P's near unity selectivity toward NH₃ under mild conditions, while Ni had almost no conversion of NO₃⁻.³⁸ This confirms the importance of a multi-elemental catalyst and motivates the investigation of nickel phosphide materials as electrocatalysts for NO₃RR. Although previous theoretical work on Ni₂P electrocatalysts for NO₃RR has highlighted the critical role of Ni₂P's ability to co-adsorb NO₃⁻ and H,^{20,24} corroborating experimental data has not yet been reported. In this study, we investigate the nitrate reduction behavior of Ni₂P nanocrystals as a case study for elucidating the role of metal phosphide active site ensembles on NO₃⁻ reduction behavior. Our rate order analysis suggests a competitive Langmuir-Hinshelwood mechanism, which we use to understand the selectivity of Ni₂P for nitrate reduction over a range of reductive potentials.

Ni₂P nanocrystals were prepared according to previous methods developed in our group.³⁹ Briefly, NiCl₂ was added to oleylamine and degassed at 120 °C for 1 hour. The temperature was lowered to 50 °C, tris(diethylamino) phosphine was injected, and the temperature was raised to 250 °C and held for 1 hour. X-ray diffraction (XRD) and transmission electron microscopy (TEM) measurements show monodisperse, 5.4 ± 0.8 nm nanocrystals (Fig. S3). Ni₂P nanocrystals were deposited onto Vulcan carbon (Ni₂P/C) to prevent aggregation during annealing with slight modifications from previous methods (see SI).⁴⁰ The nanocrystals were kept under inert conditions at all

^a Department of Chemistry, University of Washington, Seattle, WA 98195, United States. Email: cossairt@uw.edu

^b Pacific Northwest National Laboratory, Richland, Washington, WA 99352, United States.

^c Department of Chemical Engineering, University of Washington, Seattle, WA 98195, United States.

Electronic Supplementary Information (ESI) available: experimental and computational methods, supplementary data, acknowledgements. See DOI: 10.1039/x0xx00000x

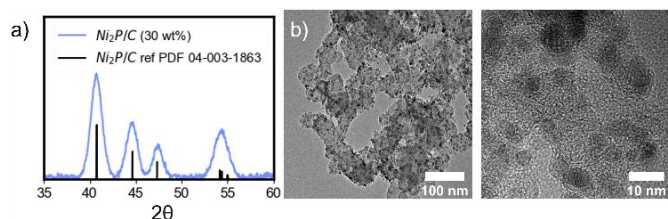


Fig. 1 a) XRD and **b)** TEM images of Ni₂P nanocrystals deposited on Vulcan carbon and annealed (Ni₂P/C).

times to prevent surface oxidation before electrocatalytic measurements. XRD and TEM measurements of Ni₂P/C demonstrate the retention of the Ni₂P crystal structure post-annealing with mild ripening to 5.8 ± 1.5 nm (**Fig. 1**). Fourier transform analysis of the particle lattice fringes reveals predominantly (111)-faceted nanocrystals after the annealing treatment (**Fig. S6**). The Ni₂P/C powder was drop-cast onto carbon paper electrodes (90 mg of Ni₂P) for electrocatalytic measurements (**Fig. S5**). All electrochemical measurements were performed in an H-cell with a 0.1 M phosphate buffer electrolyte (1:1 KH₂PO₄/K₂HPO₄, pH = 6.9).

We performed cyclic voltammetry using Ni₂P/C with varying concentrations of KNO₃ to demonstrate Ni₂P/C's activity for NO₃RR (**Fig. 2a**). We attribute the two features to the catalytic activity being mediated by two different sources: H₂PO₄ and H₂O. With 0 mM KNO₃, we can isolate the catalytic activity to the HER. Under these conditions, HER activity first exhibits a diffusion-limited response near -0.3 V due to the H-source being H₂PO₄⁻ ($pK_{a_{H_2PO_4^-}} < pK_{a_{H_2O}}$). As the potential increases and the water dissociation potential is reached, the HER current resembles the expected catalytic wave, indicating that the H-source is H₂O.⁴¹ As the concentration of KNO₃ is increased, we observe diffusion-limited NO₃RR at low cathodic potentials in the phosphate-mediated region. In both regions, there is a decrease in onset potential and an increase in current density associated with an increased concentration of KNO₃, demonstrating Ni₂P/C's activity for NO₃RR.

Varying the concentration of KNO₃ allows for determining the nitrate rate order over a range of potentials, which provides insight into the adsorbate dynamics on the catalyst surface (**Fig. 2b**).⁴¹ The NO₃⁻ rate orders were extracted from the logarithmic relationship between the current at a given potential and the concentration of KNO₃ (**Fig. S9**). In the H₂O-mediated region (< -0.25 V, highlighted in blue in **Fig. 2b**), we observe an inverted-parabolic shape, which suggests that NO₃RR is proceeding via a Langmuir-Hinshelwood mechanism^{41,42}, where adsorbed hydrogen (H*) and nitrogenous species (NO_x*) are co-adsorbed intermediates, and the coverage ratio between the two dictates selectivity between NO₃RR and HER. This conclusion assumes that the rate-limiting step is the reduction of NO₃* to NO₂*, which has been proposed in previous studies.^{14,43} The potential of maximum rate order (-0.5 V) occurs when the H*:NO_x* coverage ratio is optimized for selective NO₃⁻ reduction.⁴¹ This potential appears more negative for Ni₂P than previously measured for Cu and Ni foils,⁴¹ suggesting that Ni₂P can suppress HER over a wider potential window. We propose that Ni₂P's active site ensembles enable more optimal relative binding of H* and NO_x*, which is reflected by the shift in the

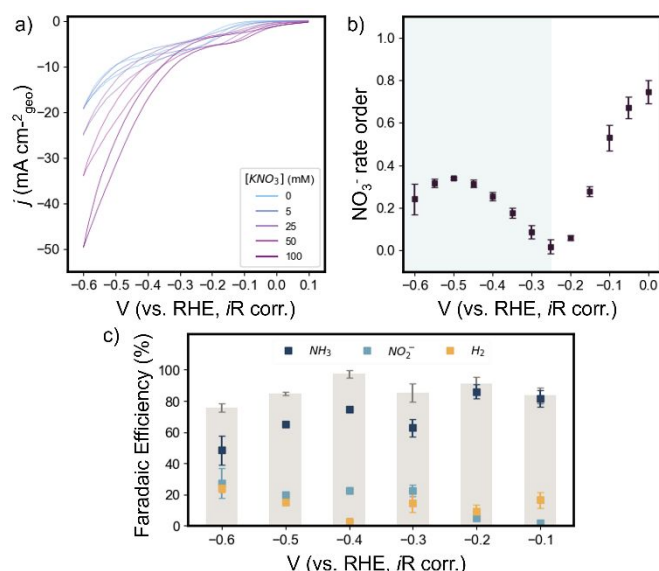


Fig. 2 a) Cyclic voltammograms of Ni₂P/C in 0.1 M KH₂PO₄/K₂HPO₄ buffer at a series of KNO₃ concentrations. **b)** Potential-dependent NO₃⁻ rate order. The region highlighted in blue (<-0.25 V) indicates a competitive Langmuir-Hinshelwood mechanism. **c)** Potential-dependent selectivity with 100 mM of KNO₃.

potential of maximum rate order to more cathodic potentials. We also observe a decreasing NO₃⁻ rate order in the phosphate-mediated region (>-0.25 V) as we move to more negative potentials. We attribute this decrease to the rate being limited by H₂PO₄⁻ ([H⁺] or coverage of H*) instead of NO₃⁻, which is supported by the presence of the H₂PO₄⁻ deprotonation peak in **Fig. 2a**. This rate order analysis assumes that the rate of NO₃RR and HER are independent; however, assuming they are dependent results in identical conclusions (**Fig. S9**).

The rate order analysis supports our hypothesis that Ni₂P/C can simultaneously co-adsorb multiple intermediates required to reduce NO₃⁻ to NH₃. To investigate how this influences the selectivity of NO₃RR, we conducted chronoamperometry experiments and quantified the products (**Fig. 2c, S9, S10a**). NH₃ and NO₂⁻ were quantified with previously reported UV-visible colorimetric methods (**Fig. S1–S2**, see SI). After considering three possible reaction pathways for NO₃RR to ammonia^{15,44}, DFT calculations suggest that NH₃ is formed by an 8e⁻ sequential deoxygenation and hydrogenation pathway with a NO₂⁻ intermediate (**Fig. S13–14**). *In situ* mass spectrometry measurements confirmed that the sole gaseous product is H₂ at -0.6 V from the competing HER (**Fig. S11**). We believe H₂ is the sole gaseous product over the entire range of potentials due to the lack of N₂ and N₂O (which should have more sluggish kinetics than the other thermodynamically accessible products) at the most cathodic potential in the series. Bulk electrolysis results reveal that Ni₂P/C has >60% Faradaic efficiency (FE) toward NO₃RR at all tested potentials and nearly 100% FE at -0.4 V. As potential decreases, NH₃ selectivity decreases and the production of H₂ and NO₂⁻ increases. We propose that the reaction selectivity is dictated by the ratio of H* and NO_x* on the surface, which is tuned by the applied potential. At low cathodic potentials (≥ -0.2 V) where NO₃⁻ reduction is mediated by H₂PO₄⁻, we observe >80% NH₃ FE and 15–20% H₂ FE, with

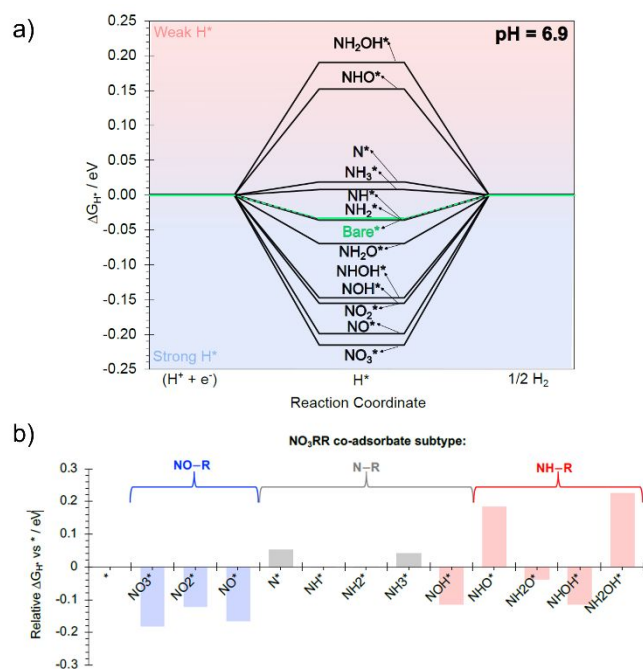


Fig. 3 a) Calculated free energy profile at 0.00 V vs. RHE, pH = 6.9, and 300 K for the adsorption of H* onto the Ni₃ hollow site of the Ni₃P₂ terminated surface, with and without surface functional groups. **b)** Plot showing the relative hydrogen adsorption free energy as a function of co-adsorbed species relative to ΔG_{H^*} on the bare Ni₂P surface (*), at pH = 6.9 and T = 300 K. The colors correspond to the co-adsorbate subtypes consisting of NO-R (blue), N-R (grey) and NH-R (red) containing species.

minimal NO_2^- production. We propose that the diffusion-limited nature of $H_2PO_4^-$ allows NO_x^* to saturate the surface and decreases the ratio of $H^*:NO_x^*$. This coverage ratio favors the hydrogenation of NO_x^* species to NH_3 over the formation of NO_2^- and H_2 .^{45,46} In the H_2O -mediated region (≤ -0.3 V), we observe near 100% FE toward NO_3RR at -0.4 V, which suggests a surface coverage that almost completely inhibits HER activity, i.e., an ideal ratio of $H^*:NO_x^*$ for selectively performing NO_3RR . Deviation from the ideal $H^*:NO_x^*$ ratio results in lower NO_3RR selectivity. At -0.3V, we observe a rise in NO_2^- selectivity relative to -0.2 V due to $H^*:NO_x^*$ being too low. Conversely, as potentials become more cathodic of -0.4 V, the $H^*:NO_x^*$ ratio increases and favors H_2 formation by promoting H-H coupling over NO_x^* hydrogenation, decreasing overall NO_3RR selectivity.

Complementary to the experiments, we also performed DFT calculations on a Ni₂P surface to disentangle the influence of NO_x^* and H* co-adsorption on their respective energetics and reaction selectivity. Systematic exploration of various nitrogenous species reveals that co-adsorption of nitrogenous species and H* modulates ΔG_{H^*} , the key binding mode of nitrogenous species, and the overall free energy profile of the reaction (Fig. 3, S14b–15, see SI), which is consistent with previous work.⁴⁷ ΔG_{H^*} can be modulated by as much as 0.040 eV, where oxygenated, unhydrogenated nitrogenous species (i.e., NO_3^* , NO_2^*) strengthen ΔG_{H^*} .

We hypothesize that stronger values of ΔG_{H^*} may direct Ni₂P/C's selectivity toward NH_3 even at negative reductive potentials (i.e., -0.6 V). At these potentials, despite a strong driving force toward HER, NO_x^* intermediates could be

strengthening the adsorption of H*, which inhibits the Tafel step of HER and promotes the hydrogenation of NO_x^* .^{45,46} In general, the observed difference in ΔG due to co-adsorbed H* can be rationalized in terms of the electron-donating/withdrawing propensity and steric effects of the co-adsorbates, where in our system, the H* on a Ni₃-hollow site exhibits electrostatic repulsion effect on species such as NO_3^- and NO_2^- .^{32,48,49} The impacts of H* and NO_x^* on each other's surface energetics imply that the rates of NO_3RR and HER are inherently dependent, corroborating our conclusions from the rate-order analysis that NO_x^* and H* are co-adsorbing on Ni₂P/C's active site ensembles during NO_3RR .

This work demonstrates Ni₂P/C's activity and selectivity for NO_3RR at a range of potentials, where NO_3RR FE ranges from 60% to nearly 100%, with selectivity for NH_3 maximized in the $H_2PO_4^-$ -mediated region (> -0.25 V). DFT calculations and rate order analysis demonstrate Ni₂P/C's ability to co-adsorb nitrogenous and hydrogen intermediates and selectively produce NH_3 over the range of potentials. We rationalize the potential-dependent selectivity of Ni₂P/C by changes in the surface coverage of adsorbates, where the ratio of $H^*:NO_x^*$ at -0.4 V is ideal for performing NO_3RR over HER. This work is a case study of the importance of the active site ensembles on metal phosphide surfaces that drive nitrate reduction selectivity toward NH_3 . This motivates future work in electrocatalyst design of metal phosphides toward dictating catalytic selectivity by tuning stoichiometry, doping, and morphology.

E.N. and P.S.R. acknowledge funding from the Center for Molecular Electrocatalysis, an Energy Frontier Research Center funded by the U.S. Department of Energy, Office of Basic Energy Sciences. E.M.S., A.P., and B.R. acknowledge funding from the National Science Foundation (CBET 205227). Computational resources were provided by the National Energy Research Computing Center at LBNL. PNNL is operated by Battelle under contract number DEAC05-75RL01830.

Conflicts of interest

There are no conflicts to declare.

Notes and references

- Ammonia: zero-carbon fertiliser, fuel and energy store, *The Royal Society*, 2020, 1–40.
- N. Gruber and J. N. Galloway, *Nature*, 2008, **451**, 293–296.
- Y. Zeng, C. Priest, G. Wang and G. Wu, *Small Methods*, 2020, **4**, 2000672.
- P. H. van Langevelde, I. Katsounaros and M. T. M. Koper, *Joule*, 2021, **5**, 290–294.
- J. Li, G. Zhan, J. Yang, F. Quan, C. Mao, Y. Liu, B. Wang, F. Lei, L. Li, A. W. M. Chan, L. Xu, Y. Shi, Y. Du, W. Hao, P. K. Wong, J. Wang, S.-X. Dou, L. Zhang and J. C. Yu, *J. Am. Chem. Soc.*, 2020, **142**, 7036–7046.
- T. Chen, H. Li, H. Ma and M. T. M. Koper, *Langmuir*, 2015, **31**, 3277–3281.
- K. Chen, J. Xiang, Y. Guo, X. Liu, X. Li and K. Chu, *Nano Lett.*, 2024, **24**, 541–548.

- 8 Q. Hu, K. Yang, O. Peng, M. Li, L. Ma, S. Huang, Y. Du, Z.-X. Xu, Q. Wang, Z. Chen, M. Yang and K. P. Loh, *J. Am. Chem. Soc.*, 2024, **146**, 668–676.
- 9 J.-Q. Chen, X.-X. Ye, D. Zhou and Y.-X. Chen, *J. Phys. Chem. C*, 2023, **127**, 2918–2928.
- 10 H. Yin, F. Dong, Y. Wang, H. Su, X. Li, Y. Peng, H. Duan and J. Li, *Nano Lett.*, 2023, **23**, 11899–11906.
- 11 H. Yin, F. Dong, H. Su, Z. Zhuang, Y. Wang, D. Wang, Y. Peng and J. Li, *ACS Nano*, 2023, **17**, 25614–25624.
- 12 E. Murphy, Y. Liu, I. Matanovic, M. Rüscher, Y. Huang, A. Ly, S. Guo, W. Zang, X. Yan, A. Martini, J. Timoshenko, B. R. Cuenya, I. V. Zhenyuk, X. Pan, E. D. Spoeerke and P. Atanassov, *Nature Commun.*, 2023, **14**, 4554.
- 13 Z.-Y. Wu, M. Karamad, X. Yong, Q. Huang, D. A. Cullen, P. Zhu, C. Xia, Q. Xiao, M. Shakouri, F.-Y. Chen, J. Y. (Timothy) Kim, Y. Xia, K. Heck, Y. Hu, M. S. Wong, Q. Li, I. Gates, S. Siahrostami and H. Wang, *Nature Commun.*, 2021, **12**, 2870.
- 14 J.-X. Liu, D. Richards, N. Singh and B. R. Goldsmith, *ACS Catal.*, 2019, **9**, 7052–7064.
- 15 T. Hu, C. Wang, M. Wang, C. M. Li and C. Guo, *ACS Catal.*, 2021, **11**, 14417–14427.
- 16 X. Lu, H. Song, J. Cai and S. Lu, *Electrochem. Commun.*, 2021, **129**, 107094.
- 17 J. Ni, J. Yan, F. Li, H. Qi, Q. Xu, C. Su, L. Sun, H. Sun, J. Ding and B. Liu, *Adv. Energy Mater.*, 2024, **n/a**, 2400065.
- 18 Q. Liu, Y. Lin, S. Gu, Z. Cheng, L. Xie, S. Sun, L. Zhang, Y. Luo, A. A. Alshehri, M. S. Hamdy, Q. Kong, J. Wang and X. Sun, *Nano Res.*, 2022, **15**, 7134–7138.
- 19 G. Wang, Y. Zhang, K. Chen, Y. Guo and K. Chu, *Inorg. Chem.*, 2023, **62**, 6570–6575.
- 20 Q. Yao, J. Chen, S. Xiao, Y. Zhang and X. Zhou, *ACS Appl. Mater. Interfaces*, 2021, **13**, 30458–30467.
- 21 Q.-L. Hong, J. Zhou, Q.-G. Zhai, Y.-C. Jiang, M.-C. Hu, X. Xiao, S.-N. Li and Y. Chen, *Chem. Commun.*, 2021, **57**, 11621–11624.
- 22 Y. Jia, Y.-G. Ji, Q. Xue, F.-M. Li, G.-T. Zhao, P.-J. Jin, S.-N. Li and Y. Chen, *ACS Appl. Mater. Interfaces*, 2021, **13**, 45521–45527.
- 23 R. Zhang, Y. Guo, S. Zhang, D. Chen, Y. Zhao, Z. Huang, L. Ma, P. Li, Q. Yang, G. Liang and C. Zhi, *Adv. Energy Mater.*, 2022, **12**, 2103872.
- 24 S. Huo, S. Yang, Q. Niu, Z. Song, F. Yang and L. Song, *ChemCatChem*, 2020, **12**, 4600–4610.
- 25 L. Wen, Y. Sun, C. Zhang, J. Yu, X. Li, X. Lyu, W. Cai and Y. Li, *ACS Appl. Energy Mater.*, 2018, **1**, 3835–3842.
- 26 B. Liu, X. Lan, Q. Zhong and T. Wang, *ACS Catal.*, 2024, **14**, 757–775.
- 27 D.-Y. Kuo, E. Nishiwaki, R. A. Rivera-Maldonado and B. M. Cossairt, *ACS Catal.*, 2023, **13**, 287–295.
- 28 P. Liu and J. A. Rodriguez, *J. Am. Chem. Soc.*, 2005, **127**, 14871–14878.
- 29 E. J. Popczun, J. R. McKone, C. G. Read, A. J. Biacchi, A. M. Wiltrout, N. S. Lewis and R. E. Schaak, *J. Am. Chem. Soc.*, 2013, **135**, 9267–9270.
- 30 B. Seo, D. San Baek, Y. Jin Sa and S. Hoon Joo, *CrystEngComm*, 2016, **18**, 6083–6089.
- 31 C. A. Downes, K. M. Van Allsburg, S. A. Tacey, K. A. Unocic, F. G. Baddour, D. A. Ruddy, N. J. Libretto, M. M. O'Connor, C. A. Farberow, J. A. Schaidle and S. E. Habas, *Chem. Mater.*, 2022, **34**, 6255–6267.
- 32 I. A. Murphy, P. S. Rice, M. Monahan, L. P. Zasada, E. M. Miller, S. Raugei and B. M. Cossairt, *Chem. Mater.*, 2021, **33**, 9652–9665.
- 33 S. Banerjee, A. Kakekhani, R. B. Wexler and A. M. Rappe, *ACS Catal.*, 2021, **11**, 11706–11715.
- 34 K. U. D. Calvino, A. W. Alherz, K. M. K. Yap, A. B. Laursen, S. Hwang, Z. J. L. Bare, Z. Clifford, C. B. Musgrave and G. C. Dismukes, *J. Am. Chem. Soc.*, 2021, **143**, 21275–21285.
- 35 K. U. D. Calvino, A. B. Laursen, K. M. K. Yap, T. A. Goetjen, S. Hwang, N. Murali, B. Mejia-Sosa, A. Lubarski, K. M. Teeluck, E. S. Hall, E. Garfunkel, M. Greenblatt and G. C. Dismukes, *Energy Environ. Sci.*, 2018, **11**, 2550–2559.
- 36 M. S. Duyar, A. Gallo, S. K. Regli, J. L. Snider, J. A. Singh, E. Valle, J. McEnaney, S. F. Bent, M. Rønning and T. F. Jaramillo, *Catalysts*, 2021, **11**, 143.
- 37 C. A. Downes, N. J. Libretto, A. E. Harman-Ware, R. M. Happs, D. A. Ruddy, F. G. Baddour, J. R. Ferrell III, S. E. Habas and J. A. Schaidle, *ACS Appl. Energy Mater.*, 2020, **3**, 10435–10446.
- 38 L. Wei, D.-J. Liu, B. A. Rosales, J. W. Evans and J. Vela, *ACS Catal.*, 2020, **10**, 3618–3628.
- 39 M. E. Mundy, D. Ung, N. L. Lai, E. P. Jahrman, G. T. Seidler and B. M. Cossairt, *Chem. Mater.*, 2018, **30**, 5373–5379.
- 40 F. G. Baddour, E. J. Roberts, A. T. To, L. Wang, S. E. Habas, D. A. Ruddy, N. M. Bedford, J. Wright, C. P. Nash, J. A. Schaidle, R. L. Brutchey and N. Malmstadt, *J. Am. Chem. Soc.*, 2020, **142**, 1010–1019.
- 41 O. Q. Carvalho, R. Marks, H. K. K. Nguyen, M. E. Vitale-Sullivan, S. C. Martinez, L. Árnadóttir and K. A. Stoerzinger, *J. Am. Chem. Soc.*, 2022, **144**, 14809–14818.
- 42 N. Singh, U. Sanyal, G. Ruehl, K. A. Stoerzinger, O. Y. Gutiérrez, D. M. Camaioni, J. L. Fulton, J. A. Lercher and C. T. Campbell, *Journal of Catalysis*, 2020, **382**, 372–384.
- 43 Z. Wang, D. Richards and N. Singh, *Catal. Sci. Technol.*, 2021, **11**, 705–725.
- 44 Y. Cao, S. Yuan, L. Meng, Y. Wang, Y. Hai, S. Su, W. Ding, Z. Liu, X. Li and M. Luo, *ACS Sustainable Chem. Eng.*, 2023, **11**, 7965–7985.
- 45 K. Yang, S.-H. Han, C. Cheng, C. Guo, T. Li and Y. Yu, *J. Am. Chem. Soc.*, 2024, **146**, 12976–12983.
- 46 Y. Xiong, Y. Wang, J. Zhou, F. Liu, F. Hao and Z. Fan, *Adv. Mater.*, 2024, **36**, 2304021.
- 47 H. Yuan, N. Sun, J. Chen, J. Jin, H. Wang and P. Hu, *ACS Catal.*, 2018, **8**, 9269–9279.
- 48 P. S. Rice, Y. Mao, C. Guo and P. Hu, *Phys. Chem. Chem. Phys.*, 2019, **21**, 5932–5940.
- 49 P. S. Rice, Z.-P. Liu and P. Hu, *J. Phys. Chem. Lett.*, 2021, **12**, 10637–10645.